molecular pharmaceutics

articles

Noninvasive Monitoring of the Fate of ^{111}In-Labeled Block Copolymer Micelles by High Resolution and High Sensitivity MicroSPECT/CT Imaging

Bryan Hoang,[†] Helen Lee,[†] Raymond M. Reilly,[†,‡,||] and Christine Allen*[,†,§]

Departments of Pharmaceutical Sciences, Chemistry, and Medical Imaging, University of Toronto, Toronto, ON, Canada, and Toronto General Research Institute, University Health Network, Toronto, ON, Canada

Received November 23, 2008; Revised Manuscript Received January 27, 2009; Accepted February 2, 2009

Abstract: The validation of high sensitivity and high resolution microSPECT/CT imaging for tracking the *in vivo* pathway and fate of an ^{111}Indium-labeled (^{111}In) amphiphilic diblock copolymer micelle formulation is presented. Heterobifunctional poly(ethylene glycol) was used to initiate cationic ring opening polymerization of ε-caprolactone, which was then conjugated to 2-(4-isothiocyanatobenzyl)-diethylene-triaminepentaacetic acid (*p*-SCN-Bn-DTPA) for chelation with ^{111}In. The micelles were characterized in terms of their physicochemical properties including size, size distribution, zeta-potential, and radiochemical purity. Elimination kinetics and tissue deposition were evaluated in healthy mice following administration of ^{111}In-micelles, ^{111}In-DTPA-*b*-PCL unimers (i.e., administered under the critical micelle concentration) or ^{111}In-Bn-DTPA. Healthy and MDA-MB-231 tumor-bearing mice were imaged using microSPECT/CT following iv administration of ^{111}In-micelles or ^{111}In-Bn-DTPA. Overall, incorporation of ^{111}In onto the surface of thermodynamically stable micelles results in long plasma residence times for the radionuclide and preferential localization within the spleen (22 $\pm$ 5% i.d./g), liver (13 $\pm$ 3% i.d./g), and tumor (9 $\pm$ 2% i.d./g). MicroSPECT/CT imaging provided noninvasive longitudinal visualization of circulation dynamics and tissue deposition. A strong correlation between image-based region of interest (ROI) analysis and biodistribution data was found, implying that nuclear imaging can be used as a noninvasive tool to accurately quantify tissue distribution. As well, the image-based assessment provided unique insight into the intratumoral distribution of the micelles *in vivo*.

Keywords: Polymeric micelles; amphiphilic diblock copolymers; ^{111}indium; nuclear imaging; SPECT/CT

Introduction

Nanotechnology has far-reaching implications in several branches of medicine including oncology, diagnostic radiology, and nuclear medicine. In oncology the impact of nanotechnology is evidenced by the large number of anticancer drugs that have reached late stage clinical development and rely on formulation in nanosized delivery systems.[1] As well, several nanotechnologies have shown promise in cancer imaging and diagnostic applications such as disease detection, characterization, and staging (e.g., Fenestra).[2−4] The toolbox of nanotechnologies commonly explored for oncologic applications includes liposomes,[5,6] lipid micelles,[7,8] nanoemulsions,[9] carbon nanotubes,[10] poly-

* Corresponding author. Mailing address: Leslie Dan Faculty of Pharmacy, University of Toronto, 144 College St., Toronto, ON, Canada, M5S 3M2. Phone: (416) 946-8594. Fax: (416) 978-8511. E-mail: cj.allen@utoronto.ca.

† Department of Pharmaceutical Sciences, University of Toronto, Toronto, ON, Canada.

‡ Department of Medical Imaging, University of Toronto, Toronto, ON, Canada.

§ Department of Chemistry, University of Toronto, Toronto, ON, Canada.

|| Toronto General Research Institute, University Health Network, Toronto, ON, Canada.

(1) Lim Soo, P.; Dunne, M.; Liu, J.; Allen, C. Nano-Sized Colloidal Particles as Parenteral Formulation Strategies for Hydrophobic Anti-Cancer Agents. In *Nanotechnology in Drug Delivery*; S. Science/AAPS: 2008.

(2) Mitra, A.; Nan, A.; Line, B. R.; Ghandehari, H. Nanocarriers for nuclear imaging and radiotherapy of cancer. *Curr. Pharm. Des.* **2006**, *12*, 4729–4749.

(3) Torchilin, V. P. Targeted pharmaceutical nanocarriers for cancer therapy and imaging. *AAPS J.* **2007**, *9*, E128–E147.

10.1021/mp8002418 CCC: $40.75
Published on Web 02/02/2009

meric nanospheres,[11,12] gold nanoparticles,[13] and block copolymer micelles.[14]

Block copolymer micelles are one of the nanotechnologies that has been explored for both therapeutic[14−18] and imaging applications.[19−22] In aqueous media, micelles appear as nanosized assemblies of amphiphilic copolymers with a hydrophobic core surrounded by a hydrophilic corona.[23] The distinct hydrophilic and hydrophobic domains allow for incorporation of lipophilic material within the core (i.e., drugs, contrast agents), amphiphilic material at the core−corona interface, and conjugation of hydrophilic moieties to the corona. One of the unique advantages of block copolymer micelles is that their physicochemical characteristics such as size, morphology, and thermodynamic and kinetic stability can be manipulated to suit a potential application through modifications to the copolymer composition.[23−25] Also, the colloidal nature or size of block copolymer micelles, and other nanosized vehicles, facilitates their retention within the circulation for prolonged periods, in comparison to low molecular weight small molecules.[26,27] Stable vehicles with prolonged retention in the circulation may be employed for passive and active targeting to tumor sites. Indeed, studies have shown that a size of less than 100 nm and the presence of a nonionic, steric-stabilizing hydrophilic shell at the vehicle surface can reduce uptake by the mononuclear phagocyte system (MPS).[28,29] The reduced MPS uptake and prolonged circulation time are crucial for passive targeting of these nanosized vehicles to inflamed tissues or tumors

(4) Graham, K. C.; Ford, N. L.; MacKenzie, L. T.; Postenka, C. O.; Groom, A. C.; MacDonald, I. C.; Holdsworth, D. W.; Drangova, M.; Chambers, A. F. Noninvasive quantification of tumor volume in preclinical liver metastasis models using contrast-enhanced X-ray computed tomography. *Invest. Radiol.* **2008**, *43*, 92–99.

(5) Parnham, M. J. Liposomes in biomedical research. *Drug News Perspect.* **1994**, *7*, 574–576.

(6) Schwendener, R. A. Liposomes in biology and medicine. *Adv. Exp. Med. Biol.* **2007**, *620*, 117–128.

(7) Torchilin, V. P. Lipid-core micelles for targeted drug delivery. *Curr. Drug Delivery* **2005**, *2*, 319–327.

(8) Wang, J.; Mongayt, D.; Torchilin, V. P. Polymeric micelles for delivery of poorly soluble drugs: Preparation and anticancer activity in vitro of paclitaxel incorporated into mixed micelles based on poly(ethylene glycol)-lipid conjugate and positively charged lipids. *J. Drug Target.* **2005**, *13*, 73–80.

(9) Fronza, T.; Campos, A.; Teixeira, H. Nanoemulsions as delivery systems for ophthalmic drugs. *Acta Farm. Bonaerense* **2004**, *23*, 558–566.

(10) Yang, W.; Thordarson, P.; Gooding, J. J.; Ringer, S. P.; Braet, F. Carbon nanotubes for biological and biomedical applications. *Nanotechnology* **2007**, *18*, 1–12.

(11) Feng, S. S.; Mu, L.; Chen, B. H.; Pack, D. Polymeric nanospheres fabricated with natural emulsifiers for clinical administration of an anticancer drug paclitaxel (Taxol®). *Mater. Sci. Eng., C* **2002**, *20*, 85–92.

(12) Gref, R.; Minamitake, Y.; Peracchia, M. T.; Trubetskoy, V.; Torchilin, V.; Langer, R. Biodegradable long-circulating polymeric nanospheres. *Science* **1994**, *263*, 1600–1603.

(13) Chen, M.; Yamamuro, S.; Farrell, D.; Majetich, S. A. Gold-coated iron nanoparticles for biomedical applications. *J. Appl. Phys.* **2003**, *93*, 7551–7553.

(14) Gaucher, G.; Dufresne, M. H.; Sant, V. P.; Kang, N.; Maysinger, D.; Leroux, J. C. Block copolymer micelles: Preparation, characterization and application in drug delivery. *J. Controlled Release* **2005**, *109*, 169–188.

(15) Hamaguchi, T.; Matsumura, Y.; Suzuki, M.; Shimizu, K.; Goda, R.; Nakamura, I.; Nakatomi, I.; Yokoyama, M.; Kataoka, K.; Kakizoe, T. NK105, a paclitaxel-incorporating micellar nanoparticle formulation, can extend in vivo antitumour activity and reduce the neurotoxicity of paclitaxel. *Br. J. Cancer* **2005**, *92*, 1240–1246.

(16) Harada, A.; Kataoka, K. Supramolecular assemblies of block copolymers in aqueous media as nanocontainers relevant to biological applications. *Prog. Polym. Sci.* **2006**, *31*, 949–982.

(17) Kabanov, A. V.; Batrakova, E. V.; Alakhov, V. Y. Pluronic (R) block copolymers as novel polymer therapeutics for drug and gene delivery. *J. Controlled Release* **2002**, *82*, 189–212.

(18) Liu, J.; Lee, H.; Allen, C. Formulation of drugs in block copolymer micelles: drug loading and release. *Curr. Pharm. Des.* **2006**, *12*, 4685–4701.

(19) Hong, G.; Yuan, R.; Liang, B.; Shen, J.; Yang, X.; Shuai, X. Folate-functionalized polymeric micelles as hepatic carcinoma-targeted, MRI-ultrasensitive delivery system of antitumor drugs. *Biomed. Microdevices* **2008**, 1–8.

(20) Park, Y. J.; Lee, J. Y.; Chang, Y. S.; Jeong, J. M.; Chung, J. K.; Lee, M. C.; Park, K. B.; Lee, S. J. Radioisotope carrying polyethylene oxide-polycaprolactone copolymer micelles for targetable bone imaging. *Biomaterials* **2002**, *23*, 873–879.

(21) Torchilin, V. P. PEG-based micelles as carriers of contrast agents for different imaging modalities. *Adv. Drug Delivery Rev.* **2002**, *54*, 235–252.

(22) Yang, Z.; Zheng, S.; Harrison, W. J.; Harder, J.; Wen, X.; Gelovani, J. F.; Qiao, A.; Li, C. Long-circulating near-infrared fluorescence core-cross-linked polymeric micelles: Synthesis, characterization, and dual nuclear/optical imaging. *Biomacromolecules* **2007**, *8*, 3422–3428.

(23) Allen, C.; Maysinger, D.; Eisenberg, A. Nanoengineering block copolymer aggregates for drug delivery. *Colloids Surf., B* **1999**, *16*, 3–27.

(24) Kwon, G. S.; Kataoka, K. Block copolymer micelles as long-circulating drug vehicles. *Adv. Drug Delivery Rev.* **1995**, *16*, 295–309.

(25) Liu, J.; Zeng, F.; Allen, C. In vivo fate of unimers and micelles of a poly(ethylene glycol)-block-poly(caprolactone) copolymer in mice following intravenous administration. *Eur. J. Pharm. Biopharm.* **2007**, *65*, 309–319.

(26) Dreher, M. R.; Liu, W. G.; Michelich, C. R.; Dewhirst, M. W.; Yuan, F.; Chilkoti, A. Tumor vascular permeability, accumulation, and penetration of macromolecular drug carriers. *J. Natl. Cancer Inst.* **2006**, *98*, 335–344.

(27) Kim, S. Y. Preparation and characterization of biodegradable nanospheres composed of methoxy poly(ethylene Glycol) and DL-lactide block copolymer as novel drug carriers. *J. Controlled Release* **1998**, *56*, 197–208.

(28) Allen, C.; Dos Santos, N.; Gallagher, R.; Chiu, G. N.; Shu, Y.; Li, W. M.; Johnstone, S. A.; Janoff, A. S.; Mayer, L. D.; Webb, M. S.; Bally, M. B. Controlling the physical behaviour and biological performance of liposome formulations through use of surface grafted poly(ethylene glycol). *Biosci. Rep.* **2002**, *22*, 225–250.

(29) Allen, T. M.; Hansen, C. Pharmacokinetics of stealth versus conventional liposomes: effect of dose. *Biochem. Biophys. Acta.* **1991**, *1068*, 133–141.

which have "leaky" vasculature via the enhanced permeation and retention (EPR) effect.[30]

In recent years, invaluable insight on the pathway and fate of drug delivery systems *in vivo* has been gained through the use of noninvasive imaging techniques.[31−34] The unique information emerging from these studies enables optimization of the delivery system and may accelerate drug development efforts. As well, the incorporation of an imageable component into a drug delivery system creates a multifunctional system that permits pursuit of image-guided drug delivery for real-time monitoring of tumor accumulation, intratumoral distribution, and kinetics of drug release *in vivo*. In the future such multifunctional delivery systems may be used to direct the design of personalized therapies and ultimately lead to significant improvements in treatment outcomes. In this study amphiphilic diblock copolymers were labeled with the radionuclide indium-111 (^{111}In) in order to create a system that enables real-time and noninvasive evaluation of the pathway and fate of block copolymer micelles *in vivo*, using high sensitivity and high resolution microSPECT/CT imaging. The pharmacokinetics and biodistribution of the ^{111}In-labeled copolymer, administered at concentrations above and below the critical micelle concentration (CMC) of the copolymer, were evaluated using traditional methods and image-based assessment. Data obtained via conventional assessment of biodistribution was found to correlate well with that acquired using noninvasive image-based region of interest (ROI) analysis. Moreover, microSPECT/CT imaging revealed the intratumoral distribution of the micelles *in vivo* which is critical information that is unavailable through traditional assessment of biodistribution.

Experimental Procedures

Materials. Methoxy poly(ethylene glycol) (MePEG, $M_n = 5000$, $M_w/M_n = 1.06$) was purchased from Polymer Source Inc. (Montreal, QC, Canada). Hydrochloric acid (1 M, HCl in ether), triethylamine, and dimethylsulfoxide (DMSO) were purchased from Sigma Aldrich Corp. (Oakville, ON, Canada). Heterobifunctional α-hydroxy-ω-amino poly(ethylene glycol) (HO-PEG-NH_2, $M_n = 5000$, $M_w/M_n = 1.08$) was purchased from Jenkem Technology Inc. (Beijing, China). *p*-SCN-Bn-DTPA was purchased from Macrocyclics Inc. (Dallas, TX). Toluene, dichloromethane, and ε-caprolactone (ε-CL) were purchased from Sigma Aldrich (Oakville, ON, Canada), dried under calcium hydride and distilled prior to use. ^{111}In-chloride was ordered from MDS Nordion (Kanata, ON, Canada). All other materials were used as received.

Synthesis of MePEG-*b*-PCL. MePEG-*b*-PCL was prepared by metal-free cationic ring opening polymerization of ε-CL via an activated monomer mechanism in the presence of HCl−ether using an established method described elsewhere.[25,35,36] The relative degree of polymerization of the polycaprolactone (PCL) block was calculated by ^{1}H NMR analysis by comparing the integrals of characteristic methylene peaks of the PCL block at 2.31 ppm and PEG block at 3.65 ppm in the ^{1}H NMR spectrum. ^{1}H NMR assignments are as follows: the resonances assigned to the terminal methoxy protons and methylene protons of MePEG were observed at $\delta = 3.38$ ppm (3H, CH_3−O−), 3.51 ppm (2H, CH_3−O−CH_2−CH_2−) and 3.65 ppm (4H, −O−CH_2−CH_2−), respectively. The resonance for the sequence of methylene protons of the ester carbonyl moiety of PCL were observed at $\delta = 1.38$ ppm (2H, CO−CH_2−CH_2−CH_2−CH_2−CH_2−O), 1.65 ppm (4H, CO−CH_2−CH_2−CH_2−CH_2−CH_2−O), 2.31 ppm (2H, CO−CH_2−CH_2−CH_2−CH_2−CH_2−O), and 4.07 ppm (2H, CO−CH_2−CH_2−CH_2−CH_2−CH_2−O). Lastly, terminal methylene protons of PCL and MePEG were observed at $\delta = 3.70$ ppm (2H, CH_2−CH_2−OH) and 4.22 ppm (2H, O−CH_2−CH_2−O−CO), respectively.

Preparation of DTPA-PEG-*b*-PCL. Synthesis of NH_2-PEG-*b*-PCL was conducted in a similar manner to the method described for MePEG-*b*-PCL with the exception that HO-PEG-NH_2 was used as the macroinitiator (Scheme 1). The degree of polymerization of the PCL block was calculated by comparing the integrals of characteristic methylene peaks of the PCL block at 2.29 ppm and PEG block at 3.62 ppm in the ^{1}H NMR spectrum. ^{1}H NMR assignments are as follows: $\delta = 1.40$ ppm (2H, CO−CH_2−CH_2−CH_2−CH_2−CH_2−O), 1.63 ppm (4H, CO−CH_2−CH_2−CH_2−CH_2−CH_2−O), 1.97 ppm (2H, (NH_2−CH_2−CH_2), 2.29 ppm (2H, CO−CH_2−CH_2−CH_2−CH_2−CH_2−O), 3.62 ppm (4H, −O−CH_2−CH_2−), 3.69 ppm (2H, CH_2−CH_2−OH), 4.06 ppm (2H, CO−CH_2−CH_2−CH_2−CH_2−CH_2−O), and 4.22 ppm (2H, O-CH_2−CH_2−O−CO). The metal chelator *p*-SCN-Bn-DTPA was conjugated to the NH_2-PEG-*b*-PCL copolymer by reaction of the primary

(30) Torchilin, V. P. Micellar Nanocarriers: Pharmaceutical Perspectives. *Pharm. Res.* **2007**, *24*, 1–16.

(31) Yuan, F.; Leunig, M.; Huang, S. K.; Berk, D. A.; Papahadjopoulos, D.; Jain, R. K. Mirovascular permeability and interstitial penetration of sterically stabilized (stealth) liposomes in a human tumor xenograft. *Cancer Res.* **1994**, *54*, 3352–3356.

(32) Matteucci, M. L.; Anyarambhatla, G.; Rosner, G.; Azuma, C.; Fisher, P. E.; Dewhirst, M. W.; Needham, D.; Thrall, D. E. Hyperthermia increases accumulation of Technetium-99m-labeled liposomes in feline sarcomas. *Clin. Cancer Res.* **2000**, *6*, 3748–3755.

(33) Ponce, A. M.; Viglianti, B. L.; Yu, D.; Yarmolenko, P. S.; Michelich, C. R.; Woo, J.; Bally, M. B.; Dewhirst, M. W. Magnetic resonance imaging of temperature-sensitive liposome release: drug dose painting and antitumor effects. *J. Natl. Cancer Inst.* **2007**, *99*, 53–63.

(34) Chen, Q.; Tong, S.; Dewhirst, M. W.; Yan, F. Targeting tumor microvessels using doxorubicin encapsulated in a novel thermosensitive liposome. *Mol. Cancer Ther.* **2004**, *3*, 1311–1317.

(35) Kim, M. S.; Hyun, H.; Cho, Y. H.; Seo, K. S.; Jang, W. Y.; Kim, S. K.; Khang, G.; Lee, H. B. Preparation of methoxy poly(ethyleneglycol)-block-poly(caprolactone) via activated monomer mechanism and examination of micellar characterization. *Polym. Bull.* **2005**, *55*, 149–156.

(36) Lou, X. D.; Detrembleur, C.; Jerome, R. Living cationic polymerization of delta-valerolactone and synthesis of high molecular weight homopolymer and asymmetric telechelic and block copolymer. *Macromolecules* **2002**, *35*, 1190–1195.

Scheme 1. Preparation of ^{111}In-DTPA-PEG-*b*-PCL

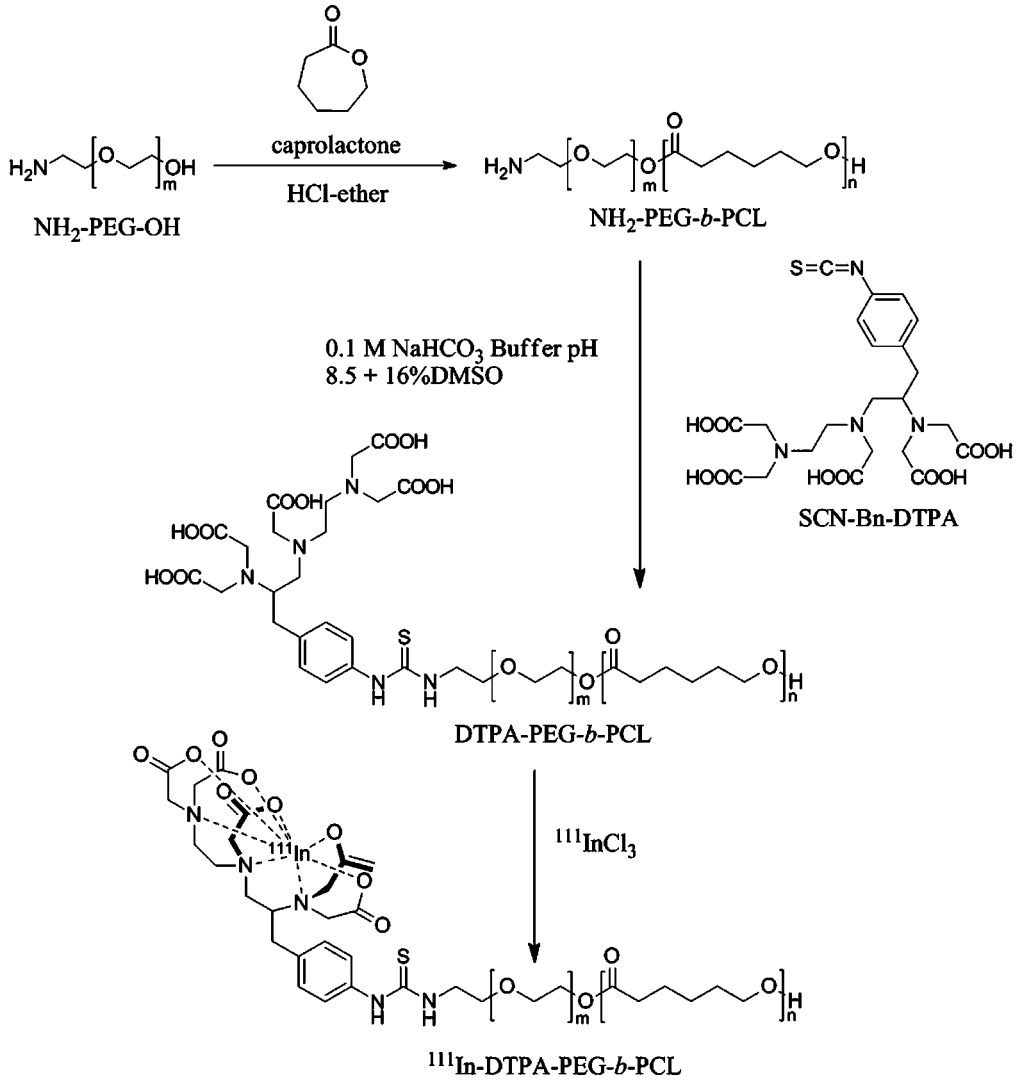

amino terminus of the copolymer with the reactive isothiocyanato group to form a highly stable thiourea complex. In a typical procedure, a 25 mg/mL solution of NH_2-PEG-*b*-PCL in sodium bicarbonate buffer (0.1 M, pH 8.5) was introduced into a vial containing a 2-fold molar excess of *p*-SCN-bn-DTPA dissolved in 16% (v/v) DMSO. The solution was stirred at room temperature for 4 h. Prior to purification to remove the unbound DTPA, an aliquot of DTPA-PEG-*b*-PCL was radiolabeled with a trace quantity of ^{111}In (<1 MBq). The DTPA conjugation efficiency was evaluated with ascending instant thin layer chromatography (ITLC) using a stationary phase of silica gel-impregnated glass fiber strips (1 × 10 cm; ITLC-SG, Pall Corp.) and a mobile phase of NaCitrate buffer (0.1 M, pH 6.0). Each strip was spotted with the sample, developed in buffer, and then sectioned for gamma-scintillation counting (γ-counter) (Wallac Wizard-1480; Perkin-Elmer Inc.). The DTPA conjugation efficiency was calculated based upon the relative amount of ^{111}In bound to DTPA-PEG-*b*-PCL in comparison to that bound to free DTPA (R_f ^{111}In-DTPA-PEG-*b*-PCL = 0.0; R_f ^{111}In-Bn-DTPA = 1.0), given the known molar ratio of DTPA to NH_2-PEG-*b*-PCL in solution.

Purification and Radiolabeling of DTPA-PEG-*b*-PCL with ^{111}In. DTPA-derivatized NH_2-PEG-*b*-PCL was purified by size exclusion chromatography using a Bio-Gel P2 column (1.5 × 30 cm column, gel exclusion limit 2 kDa; Bio-Rad Laboratories) with ddH_2O as the eluent. Fractions corresponding to the purified DTPA-PEG-*b*-PCL copolymer were collected and lyophilized. DTPA-PEG-*b*-PCL was labeled by incubation of 500 μg of the copolymer with 37 MBq of ^{111}In-acetate for 30 min at 37 °C. ^{111}In-acetate was prepared by mixing equal volumes of ^{111}In-chloride (MDS-Nordion, Inc.) with sodium acetate buffer (0.1M, pH 6.0). The radiochemical purity was evaluated by ITLC using the method previously described (R_f ^{111}In-DTPA-PEG-*b*-PCL = 0.0; R_f free ^{111}In = 1.0).

Characterization of Copolymers. ^{1}H NMR spectra were obtained on a Mercury 400 spectrometer (400 MHz for 1H) in $CDCl_3$ solvent. Chemical shifts were reported in ppm with $CDCl_3$ as the internal standard. Gel permeation chromatography (GPC) measurements were carried out at room temperature using a Waters 590 liquid chromatography system equipped with three Waters Styragel HR 4E columns

and a 410 differential refractometer detector. THF with 1% triethylamine was used as the mobile phase at a flow rate of 1.0 mL/min at 40 °C and polystyrene standards (Polysciences Inc., Warrington, PA) were used for calibration. The data obtained was analyzed using the Windows-based Millenium 2.0 software package (Waters Inc., Milford, MA). FTIR spectroscopy was conducted on a universal ATR spectrum-one Perkin-Elmer spectrophotometer (Perkin-Elmer, Connecticut, U.S.A.) with a resolution of 4 cm^{-1}. A background spectrum containing no sample was subtracted from the spectra.

Preparation and Characterization of ^{111}In-Radiolabeled Micelles. Micelles composed of MePEG-*b*-PCL were prepared by the thin-film hydration method.[37] Typically, a 50 mg sample of MePEG-*b*-PCL was dissolved in DMF by stirring at room temperature for 24 h. The copolymer solution was dried under nitrogen at room temperature and left under vacuum overnight. A 1 mL aliquot of phosphate buffered saline (PBS) (0.01 M, pH 7.4) at 60 °C was then used to hydrate the copolymer film. The solution was vortexed, stirred for 72 h at room temperature and sonicated for 1 h prior to use. ^{111}In-labeled micelles were prepared by coincubation of ^{111}In-DTPA-PEG-*b*-PCL copolymers with preformed MePEG-*b*-PCL micelles at 60 °C for 1 h and overnight at room temperature. The relative concentration of ^{111}In-labeled copolymer was calculated to be 1% of the total copolymer weight. The hydrodynamic diameter of MePEG-*b*-PCL micelles and In-DTPA-PEG-*b*-PCL micelles was determined by dynamic light scattering (DLS) at an angle of 90° and temperature of 25 °C (DynaPro-MS/X; Protein Solutions Inc., Lakewood, NJ). The samples were diluted from the original copolymer concentration of 50 mg/mL to 1 mg/mL prior to DLS measurement. For these measurements, nonradioactive $InCl_3$ (Sigma-Aldrich, St. Louis, MO) was employed and unbound $InCl_3$ was removed by dialysis. The effective mean diameter and relative size distribution of the micelles were obtained using the Dynamics V.6.7.1 Regularization algorithm (Wyatt Technology Corp.). The zeta-potential of the ^{111}In-DTPA-PEG-*b*-PCL was evaluated using a 90 Plus Particle Size Analyzer (Brookhaven Instruments Corp., New York). The acquired zeta potential measurements were analyzed using the PALS Zeta Potential Analyzer software.

***In Vitro* Stability of Micelles.** The micelle solutions were mixed with equal volumes of either PBS (0.01 M, pH 7.4) or PBS containing bovine serum albumin (45 g BSA/L in 0.01 M PBS) and incubated at 37 °C. At various time points, 20 μL aliquots of the solutions were removed and analyzed by DLS ($n = 3$) to evaluate the *in vitro* stability of the block copolymer micelles in the presence of physiologically relevant concentrations of serum protein. Transchelation of ^{111}In from ^{111}In-micelles (500 μg, 0.006 MBq/μg) to transferrin was measured *in vitro* by incubation of micelles with 1 mL of PBS or 1 mL of mouse plasma at 37 °C for up to 72 h. SEC analysis using a Superose column (1.0 × 50 cm column; GE Healthcare, QC, Canada) with PBS (0.01M, pH 7.4) as the eluent at a flow rate of 0.1 mL/min, was conducted at 24, 48, and 72 h to evaluate the dissociation of ^{111}In from the micelles. The standard transferrin peak was identified by SEC analysis of ^{111}In-transferrin, prepared by incubating ^{111}In-acetate (3 MBq) with mouse plasma for 12 h at 37 °C. An elution chromatogram was generated by counting the radioactivity in the collected fractions using a γ-counter.

Pharmacokinetics and Biodistribution. The pharmacokinetics of elimination from the blood and biodistribution of the copolymer and micelles were evaluated in healthy female BALB/c mice of 4−6 weeks of age. All animal protocols were in compliance with Canadian Council on Animal Care guidelines and following a protocol approved by the Animal Care Committee at the University Health Network (Protocol 989.5). The ^{111}In-micelles were prepared as described above. The ^{111}In-PEG-*b*-PCL unimers were prepared by direct dissolution of DTPA-PEG-*b*-PCL in PBS with vortexing, stirring at 60 °C for 1 h and room temperature overnight followed by sonication to obtain a final copolymer concentration of 20 mg/L. The DTPA-PEG-*b*-PCL unimers were then labeled with ^{111}In and the radiochemical purity was determined by ITLC as described above. Groups of 3−6 healthy female BALB/c mice (Charles River, Wilmington, MA) were administered with 3.7 MBq of ^{111}In-micelles (250 mg/kg), ^{111}In-Bn-DTPA, or ^{111}In-DTPA-PEG-*b*-PCL unimers (0.2 mg/kg) (i.e., copolymer concentration below the CMC) via iv tail vein injection. Blood samples were collected into heparin coated capillary tubes via saphenous vein puncture at regular intervals up to 48 h post injection. The samples were counted in a γ-counter and expressed as mean ± SD percent injected dose per milliliter (% i.d./mL) vs time. The mice were sacrificed 48 h post injection by cardiac puncture and the liver, spleen, heart, lungs, and kidneys were excised, weighed, counted on a γ-counter and expressed as mean ± SD percent injected dose per gram (% i.d./g) of organ. Scientist v.2.01 software (MicroMath Scientific Software, St.Louis, Missouri) was used to fit the pharmacokinetic data, using least-squares fitting parameters based upon a two-compartment, bolus input, first order output model defined by the equation

$$\text{concentration (time)} = A\, e^{-\alpha \text{time}} + B\, e^{-\beta \text{time}} \qquad (1)$$

MicroSPECT/CT Imaging of Healthy Mice. MicroSPECT/CT imaging was used as a noninvasive method to assess circulation dynamics and tissue deposition of ^{111}In. Groups of 3−4 healthy female BALB/c mice were injected with 37 MBq of ^{111}In-micelles (250 mg/kg) or ^{111}In-Bn-DTPA administered via iv tail vein injection. SPECT/CT images were acquired at 2, 4, 12, 24 and 48 h postinjection. Imaging was performed on a NanoSPECT/CT (Bioscan, Washington, DC) small animal tomography imager. The four multipinhole γ-detector heads were each fitted with nine high-resolution 1.4 mm tungsten apertures for high contrast collimation. Cone-beam CT scans (180 projections, 1

(37) Lee, H., Soo, P. L., Liu, J., Butler, M., Allen, C. Polymeric micelles for formulation of anti-cancer drugs. In *Nanotechnology in Cancer Therapy*; Amiji, M. M., Ed.; CRC Press: Boca Raton, 2006; pp 317−355.

Table 1. Characteristics of PEG and PEG-*b*-PCL Polymers Employed

	$M_{n,cal}$[a]	$M_{n,GPC}$[b]	$M_{n,NMR}$[c]	M_w/M_n[d]	CMC[e]
MePEG	–	8740	5000	1.04	–
$MePEG_{5k}$-*b*-PCL_{5k}	10000	17900	10300	1.15	38 ± 6
NH_2-PEG_{5k}-OH	–	7360	5100	1.08	–
NH_2-PEG_{5k}-*b*-PCL_{5k}	10000	18200	10100	1.14	–
DTPA-PEG_{5k}-*b*-PCL_{5k}	–	19000	11000	1.16	–

[a] $M_{n,cal} = M_{n_{PEG}} + M_{n_{PCL}}$; $M_{n_{PCL}}$ is the calculated molecular weight (Da) of the PCL block based on the feed ratio of caprolactone to MePEG. [b] $M_{n,GPC}$ is the relative molecular weight (Da) as determined by GPC with respect to poly(styrene) standards. [c] $M_{n,NMR} = M_{n_{PEG}} + M_{n_{PCL}}$; $M_{n_{PCL}}$ was calculated from ^{1}H NMR analysis. [d] M_w/M_n = polydispersity. [e] CMC = critical micelle concentration (as previously determined) (mg/L)[25].

s/projection, 45 kVp, 0.18 mA) were performed prior to helical SPECT image acquisition for anatomical reference. For helical SPECT image acquisition, 24 projections were acquired into a 512 × 512 acquisition matrix with a minimum of 100,000 counts per projection. Images were reconstructed using an ordered subset expectation maximization (OSEM) algorithm (9 iterations). Coregistration of SPECT and CT images was performed using InvivoScope software (Bioscan). Postimaging, the mice were sacrificed via cardiac puncture and the organs were excised, weighed and counted in a γ-counter. The radioactivity in the organs was quantified and compared with the relative concentration of ^{111}In in the organs estimated in the reconstructed images by region of interest (ROI) analysis. InvivoScope image processing software version 1.34 (Bioscan) was used for ROI analyses and expressed as percent injected dose per gram (% i.d./g).

MicroSPECT/CT Imaging of Tumor-Bearing Mice. Evaluation of the tumor accumulation of the ^{111}In-micelles was conducted in female athymic BALB/c mice bearing MDA-MB-231 tumor xenografts. The mice were inoculated subcutaneously in the right flank with 1×10^7 MDA-MB-231 breast cancer cells in 100 μL of growth medium mixed with 100 μL of Matrigel (BD Biosciences). Two to four weeks postinoculation, mice bearing tumors of an average volume of 150 mm^3 were administered with 37 MBq of ^{111}In-micelles (250 mg/kg) or ^{111}In-Bn-DTPA via iv tail vein injection and imaged using the NanoSPECT/CT imager at 24, 48, and 72 h post injection. Quantification was performed by ROI analysis as described above.

Statistical Analysis. All data was reported as mean ± SD. Statistical comparison of the pharmacokinetics and biodistribution of ^{111}In-micelles, ^{111}In-DTPA-PEG-*b*-PCL unimers administered under the CMC, and ^{111}In-Bn-DTPA was performed using one-way parametric analysis of variance (ANOVA) with an alpha value of 0.05. Post hoc analysis was conducted using Bonferroni's multiple comparisons test. Correlations between two variables (ROI vs biodistribution data) were calculated by generating a scatterplot (*X* versus *Y*) and tested using Pearson's correlation coefficient. All other statistical comparisons were made using the Student's *t* test. GraphPAd Prism Software v.4.0 was utilized for all statistical evaluations.

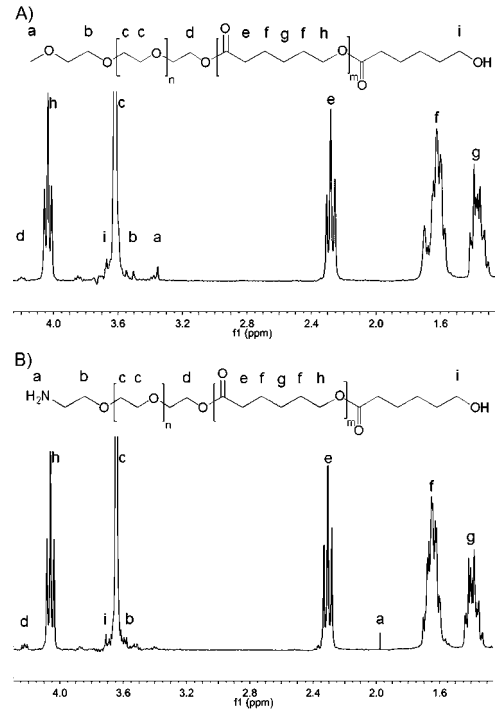

Figure 1. Structure and ^{1}H NMR spectrum with peak assignments for (A) MePEG-*b*-PCL and (B) NH_2-PEG-*b*-PCL, where *n* refers to the number of ethylene oxide repeat units and *m* the number of caprolactone repeat units.

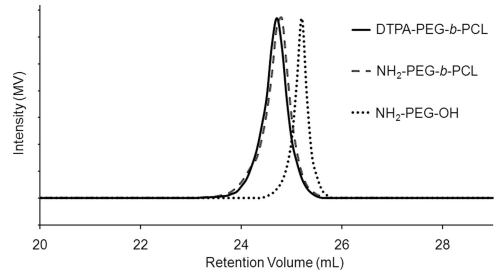

Figure 2. GPC chromatograms for NH_2-PEG-OH, NH_2-PEG-*b*-PCL, and DTPA-PEG-*b*-PCL with THF + 1% TEA as the eluent.

Results

Synthesis and Characterization of MePEG-*b*-PCL. Cationic ring opening polymerization of ε-CL via an activated monomer mechanism in the presence of HCL in ether resulted in the formation of MePEG-*b*-PCL diblock copolymers with >90% yield. The molecular weight (M_n) of the PCL block was controlled by altering the feed ratio of ε-CL to MePEG in the reaction mixture. The copolymer molecular weight was determined to be 10300 and 17900 Da by ^{1}H NMR spectroscopy and GPC analyses, respectively (Table 1). The $M_{n,NMR}$ was resolved by comparison of the integrated peak areas of the resonances at $\delta = 3.38$ ppm (MePEG) and $\delta = 2.31$ ppm (PCL) and was in good agreement with the M_n value calculated from the feed ratio of ε-CL to MePEG. Moreover, the polydispersity of the MePEG-*b*-PCL diblock copolymer was relatively narrow

(M_w/M_n =1.15) upon complete monomer conversion when compared to the MePEG macroinitiator (M_w/M_n =1.04). Figure 1A includes the ^{1}H NMR spectrum and peak assignments for the MePEG-*b*-PCL diblock copolymer.

Synthesis and Characterization of DTPA-PEG-*b*-PCL. The reactive NH_2-PEG-*b*-PCL copolymer was synthesized via cationic ring opening polymerization of ε-CL in the presence of HCL in ether. The ^{1}H NMR resonance attributable to the methylene protons of the PEG and the PCL were well resolved revealing the expected chemical structure (Figure 1B). Also, a small resonance can be observed at δ = 1.97 ppm (2H, NH_2−CH_2−CH_2−) which corresponds to the presence of the primary amine at the terminus of PEG. The absence of a definable resonance at δ = 6.17 (1H, −NH−CO−) corresponding to a secondary amine proton of an amide linkage implies that ring opening polymerization occurred via the hydroxyl endgroup of the macroinitiator.

As shown in Table 1, the M_n determined by ^{1}H NMR was in agreement with the theoretical value, indicative of successful polymerization. In addition, the polydispersity remained relatively narrow in comparison to the macroinitiator. As illustrated in Figure 2, GPC analysis reveals a shift to earlier elution times for NH_2-PEG-*b*-PCL and DTPA-PEG-*b*-PCL, relative to NH_2-PEG-OH, consistent with an increase in molecular weight distribution and indicative of successful ring opening polymerization of ε-CL and conjugation of *p*-SCN-bn-DTPA. Furthermore, monomodal molecular weight distributions were observed for the initial (NH_2-PEG-OH), intermediate (NH_2-PEG-*b*-PCL), and final products (DTPA-PEG-*b*-PCL). There was an apparent slight broadening of the GPC peaks for NH_2-PEG-*b*-PCL and DTPA-PEG-*b*-PCL compared to NH_2-PEG-OH. The discrepancy between the values obtained for the molecular weight of the copolymer from ^{1}H NMR and GPC analyses are attributed to the difference between the hydrodynamic volumes of the block copolymers and the polystyrene standards.

FTIR analysis (details in the Supporting Information Figure S1) revealed a band at 1639 cm^{-1} attributable to the bending vibrations of the terminal primary amine (N−H) group of NH_2-PEG-*b*-PCL. A band at 2867 cm^{-1} attributed to the stretching vibration of the aliphatic C−H chains of PEG can also be observed. Bands at 1730, 2950 and 3444 cm^{-1} were assigned to the stretching vibration of the carbonyl group, aliphatic C−H chain and terminal −OH group of the PCL, respectively. In addition, bands at 1100−1200 cm^{-1}, 1175 cm^{-1}, and 1346−1473 cm^{-1} corresponding to the O−C−O and C−O, the C−N, and the C−O−H bonds in the polymer backbone, respectively, were well resolved. The presence of these unique spectral characteristics indicates successful ring-opening polymerization of ε-CL by NH_2-PEG-OH in the presence of HCl in ether.

The conjugation efficiency of *p*-SCN-Bn-DTPA to NH_2-PEG-*b*-PCL was evaluated using ITLC-SG analysis of the ^{111}In-labeled reaction mixture (details in the Supporting Information Figure S2). This analysis revealed that 38.9% of the radioactivity migrated as a broad peak near the origin

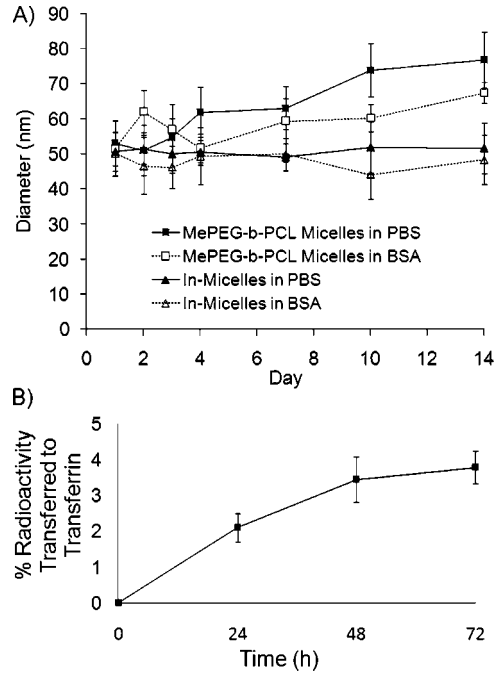

Figure 3. (A) *In vitro* stability of MePEG-*b*-PCL micelles and In-micelles in PBS or PBS containing physiologically relevant concentrations of BSA as determined by DLS. (B) Percent transchelation of ^{111}In to serum transferrin over 72 h incubation period.

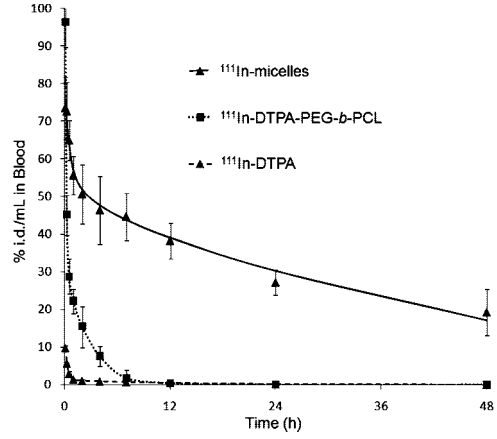

Figure 4. Percent injected dose of radioactivity remaining in the blood at various time points post injection of ^{111}In-micelles, ^{111}In-DTPA-PEG-*b*-PCL unimers administered under the CMC, or ^{111}In-Bn-DTPA.

which corresponded to ^{111}In-DTPA-PEG-*b*-PCL (fractions 1−4). The unconjugated *p*-SCN-Bn-DTPA labeled with ^{111}In (^{111}In-Bn-DTPA) migrated to the solvent front. Thus, based on the known mole ratio of *p*-SCN-Bn-DTPA:NH_2-PEG-*b*-PCL used in the reaction (2:1), it was estimated that the average number of DTPA groups conjugated per copolymer was 0.78 ± 0.09.

Purification, Radiolabeling, and Radiochemical Purity. Unconjugated *p*-SCN-Bn-DTPA was successfully removed by size exclusion chromatography using a P-2 column. The ability of this column to completely separate DTPA-PEG-*b*-PCL from unconjugated DTPA was confirmed by chro-

Table 2. Pharmacokinetic Parameters for ^{111}In-micelles, ^{111}In-DTPA-PEG-*b*-PCL Unimers or ^{111}In-Bn-DTPA Administered Intravenously in Healthy BALB/c Mice[a]

sample	$t_{1/2\alpha}$ (h)	$t_{1/2\beta}$ (h)	V_1 (mL)	V_{SS} (mL)	CL (mL/h)	AUC (% i.d. × h/mL)
^{111}In-micelles[b]	0.40	29.1	1.30	1.85	0.04	2260
^{111}In-DTPA-PEG-*b*-PCL[c]	0.09	1.99	0.60	2.32	0.94	106
^{111}In-Bn-DTPA	0.18	9.49	7.70	57.4	4.91	20.4

[a] $t_{1/2\alpha}$ = alpha half-life, $t_{1/2\beta}$ = beta half-life, V_1 = volume of distribution, V_{SS} = volume of distribution at steady-state, CL = clearance rate, AUC = area under the curve. [b] ^{111}In-Micelles refers to administration of copolymer at concentrations above CMC. [c] ^{111}In-DTPA-PEG-*b*-PCL refers to administration of copolymer at concentrations below CMC.

Table 3. Biodistribution Pattern of Radiolabeled Formulations at 48 h Postinjection in Healthy BALB/c Mice[a]

	^{111}In-Micelles	^{111}In-DTPA-PEG-*b*-PCL	^{111}In-Bn-DTPA
blood	11 ± 4	0.9 ± 0.6	0.1 ± 0.2
liver	14 ± 3	13 ± 2	0.3 ± 0.2
heart	1.4 ± 0.2	0.5 ± 0.1	0.3 ± 0.1
kidneys	3.2 ± 0.9	0.7 ± 0.2	1.7 ± 0.9
spleen	21 ± 6	2.3 ± 0.4	1.3 ± 0.5
lung	2.6 ± 0.4	0.5 ± 0.2	0.3 ± 0.1

[a] Tissue distribution in healthy mice administered ^{111}In-micelles, ^{111}In-PEG-*b*-PCL unimers administered under the CMC, or ^{111}In-Bn-DTPA 48 h p.i. (expressed as % i.d./g ± SD); representative of three-independent determinations (n = 3).

matographing this mixture labeled with ^{111}In and measuring the radioactivity of the eluted fractions in a γ-counter (details in the Supporting Information Figure S3A). ITLC analysis of DTPA-PEG-*b*-PCL following removal of unbound DTPA and labeled with ^{111}In revealed a 97 ± 2% radiochemical purity (R_f ^{111}In-DTPA-PEG-*b*-PCL = 0.0; R_f ^{111}In-Bn-DTPA = 1.0) (details in the Supporting Information Figure S3B).

Size, Size Distribution and Zeta Potential of Micelles. The mean hydrodynamic diameters of the MePEG-*b*-PCL and ^{111}In-labeled micelles were 57.7 ± 5.4 nm and 58.0 ± 5.0 nm, respectively, with monomodal size distributions (data not shown). The relative mean zeta potential of MePEG-*b*-PCL and ^{111}In-labeled micelles were found to be −2.7 and −5.8 mV, respectively.

***In Vitro* Stability.** Micelles formed from a mixture of MePEG-*b*-PCL and ^{111}In-DTPA-PEG-*b*-PCL copolymers retained their size and monomodal size distribution over the 14-day incubation period in the presence and absence of physiologically relevant concentrations of BSA (Figure 3A). Transchelation of ^{111}In from ^{111}In-micelles to transferrin was assessed *in vitro* by incubation of the ^{111}In-micelles with mouse plasma at 37 °C for 72 h (Figure 3B). Through quantification of the radioactivity in the resolved transferrin and micelle peaks by SEC analysis, it was found that transchelation to transferrin was minimal (i.e., 3.6%) over the 72 h incubation period (details in the Supporting Information Figure S4).

Pharmacokinetics and Biodistribution in Healthy Mice. The concentrations of radioactivity in the blood of mice injected intravenously with ^{111}In-micelles, ^{111}In-DTPA-*b*-PCL administered under the CMC (38 ± 6 mg/L)[25] or ^{111}In-Bn-DTPA at selected times up to 48 h p.i. are shown in Figure 4. The data was fitted using a two-compartment pharmacokinetic model; the elimination constants for the central and the peripheral compartments were obtained and are summarized in Table 2. All three radiopharmaceuticals were found to exhibit a biphasic elimination profile characterized by a rapid distribution phase and a prolonged elimination phase. The α-phase and β-phase half-lives were 4-fold and 15-fold longer, respectively, for ^{111}In-micelles compared to ^{111}In-DTPA-PEG-*b*-PCL unimers ($t_{1/2,\alpha}$ = 0.40 vs 0.09 h and $t_{1/2,\beta}$ = 29.1 vs 1.99 h, respectively; Table 2). The $t_{1/2,\beta}$ of ^{111}In-micelles was 3-fold longer than that of ^{111}In-Bn-DTPA ($t_{1/2,\beta}$ = 9.49 h). The area under the blood concentration vs time curve value for ^{111}In-micelles (AUC = 2260% i.d. × h/mL) was more than 21 times greater than that for ^{111}In-DTPA-PEG-*b*-PCL unimers (106% i.d. × h/mL) and 110-fold higher than that for ^{111}In-Bn-DTPA (AUC = 20.4% i.d. × h/mL). Taken together, these pharmacokinetic parameters revealed that ^{111}In-micelles were eliminated more slowly from the blood than ^{111}In-DTPA-PEG-*b*-PCL unimers, and much more slowly than unconjugated ^{111}In-Bn-DTPA. The volume of distribution of the central compartment (V_1) for ^{111}In-micelles (1.30 mL) was 2-fold higher than for ^{111}In-DTPA-PEG-*b*-PCL unimers (0.60 mL), but 6-fold lower than for ^{111}In-Bn-DTPA (7.70 mL). The volume of distribution at "steady-state" (V_{SS}) was slightly smaller for ^{111}In-micelles (1.85 mL) than for ^{111}In-DTPA-PEG-*b*-PCL unimers (2.32 mL), but almost 32-fold lower than that for ^{111}In-Bn-DTPA (57.4 mL). These parameters indicate that ^{111}In-micelles and ^{111}In-DTPA-PEG-*b*-PCL unimers are mainly confined to the blood volume of the mice (approximately 2−3 mL), whereas unconjugated ^{111}In-Bn-DTPA is widely distributed to tissues. At 48 h p.i., 13 ± 2% i.d./mL of the ^{111}In-micelles, 0.5 ± 0.1% i.d./mL of the ^{111}In-DTPA-PEG-*b*-PCL unimer, and 0.1 ± 0.06% i.d./mL of the ^{111}In-Bn-DTPA remained in blood circulation, respectively.

The results of biodistribution studies of the ^{111}In-micelles, ^{111}In-DTPA-PEG-*b*-PCL unimers administered under the CMC, and ^{111}In-Bn-DTPA at 48 h p.i. are shown in Table 3. Comparative biodistribution analysis revealed ^{111}In-micelles accumulated mainly in the spleen (27 ± 6% i.d./g) and liver (14 ± 3% i.d./g) in comparison to ^{111}In-DTPA-PEG-*b*-PCL unimers which exhibited a 12-fold lower spleen but similar hepatic uptake (2.3 ± 0.4% i.d./g and 13 ± 2% i.d./g, respectively). This is possibly due to mononuclear phagocyte system (MPS) clearance, commonly observed with other micelle or liposomal formulations.[25,38−41] Localization of the ^{111}In-micelles in these organs infers that the PEG corona does not completely prevent MPS uptake. The increased spleen and liver concentrations of ^{111}In-micelles over ^{111}In-DTPA-PEG-*b*-PCL unimers may be attributed to the increased blood circulation time of the copolymer in its thermodynamically stable form. Unconjugated ^{111}In-Bn-DTPA demonstrated very low uptake in these organs (1.3 ± 0.5% i.d./g and 0.3 ± 0.2% i.d./g, respectively (P <

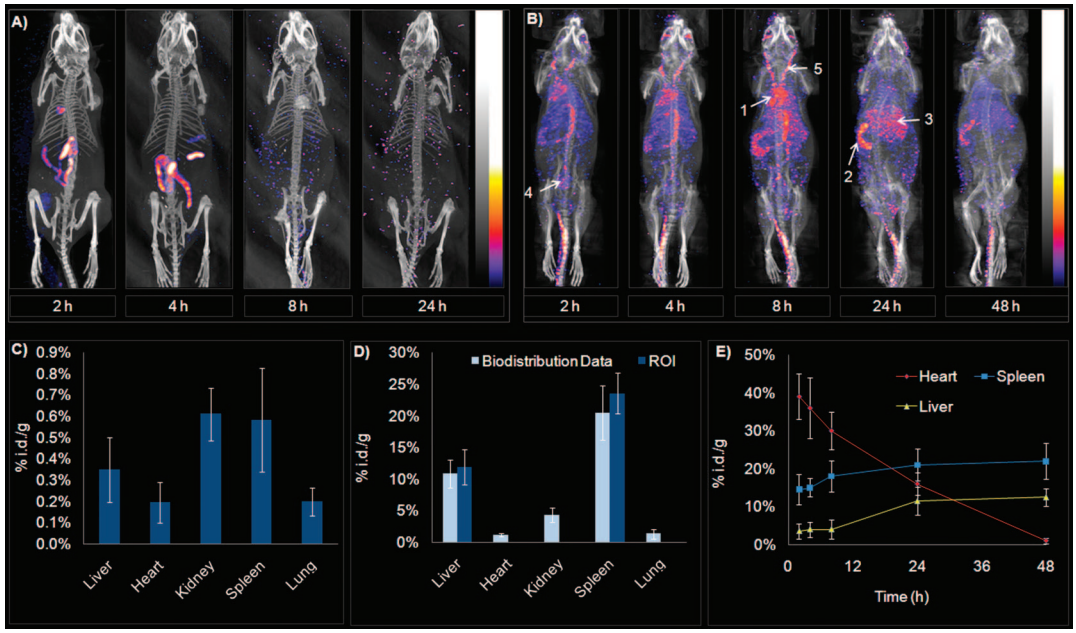

Figure 5. (A) MicroSPECT/CT maximum intensity projection (MIP) of a healthy BALB/c mouse acquired after i.v administration of ^{111}In-Bn-DTPA, which clearly delineates the G.I. tract. (B) MIP of ^{111}In-micelles in a healthy BALB/c mouse. Clear uptake is observed in the heart (1), spleen (2), liver (3), bladder (4), and carotid arteries (5) at 2 h, 4 h, 12 h, 24 h, and 48 h post injection. The ^{111}In-micelles can be observed in circulation up to 48 h p.i. (C) Postimaging biodistribution analysis, obtained by excision of organs and γ-counting, illustrating tissue uptake of ^{111}In-Bn-DTPA at 48 h p.i. (expressed as % i.d./g of organ). (D) Tissue distribution of ^{111}In-micelles by MicroSPECT/CT ROI analysis and postimaging excision of organs and γ-counting at 48 h p.i. (E) ROI analysis of heart, liver, and spleen uptake of ^{111}In-micelles in healthy BALB/c mice at various time points postinjection.

0.001)). The relatively small size of ^{111}In-Bn-DTPA resulted in rapid elimination leading to minimal normal tissue accumulation. Localization of ^{111}In-micelles and ^{111}In-DTPA-PEG-*b*-PCL unimers to other normal tissues was assumed to be nonspecific and possibly attributable to blood pool radioactivity. Accumulation in the heart and lungs were 3-fold higher for the ^{111}In-micelles than the ^{111}In-DTPA-PEG-*b*-PCL unimers, respectively. ^{111}In-Bn-DTPA demonstrated only trace accumulation in these organs (0.3 ± 0.1% i.d./g and 0.3 ± 0.1% i.d./g). Similarly, kidney accumulation was 4-fold higher for the ^{111}In-micelles than the ^{111}In-DTPA-PEG-*b*-PCL unimers (3.2 ± 0.9% i.d./g and 0.7 ± 0.2% i.d./g) and 2-fold higher than ^{111}In-Bn-DTPA (1.7 ± 0.9% i.d./g), respectively. Radioactivity remaining in the blood at 48 h p.i, (acquired via cardiac puncture) was significantly higher for ^{111}In-micelles (11 ± 4% i.d./g) in comparison to ^{111}In-DTPA-PEG-*b*-PCL unimers (0.92 ± 0.6% i.d./g) and ^{111}In-Bn-DTPA (0.12 ± 0.2% i.d./g), respectively ($p < 0.01$).

MicroSPECT/CT Imaging in Healthy Mice. As shown in Figure 5A, ^{111}In-Bn-DTPA was rapidly eliminated from the blood prior to the first imaging time point at 2 h p.i. as expected, likely by glomerular filtration but also in part by hepatobiliary elimination as noted in the microSPECT/CT images. Only some residual radioactivity that was cleared into the gastrointestinal tract was observed up to 4 h p.i. with no major accumulation of ^{111}In activity visualized in any other organs.

In contrast, as shown in Figure 5B, ^{111}In-micelles exhibited a higher level of circulating radioactivity within the heart and some major vessels. As well, radioactivity was localized in the liver, spleen and spine up to 8 h p.i. At 24 and 48 h p.i., the heart, major blood vessels, and spine could no longer be visualized but the spleen uptake became more prominent. As illustrated in Figure 5D, evaluation of the biodistribution postimaging via excision and γ-counting of organs revealed predominant spleen (24 ± 4% i.d./g), liver (13 ± 3% i.d./g), and kidney (3 ± 1% i.d./g) accumulation of the ^{111}In-micelles, while only trace accumulation in all organs excised

(38) Elbayoumi, T. A.; Torchilin, V. P. Enhanced accumulation of long-circulating liposomes modified with the nucleosome-specific monoclonal antibody 2C5 in various tumours in mice: Gamma-imaging studies. *Eur. J. Nucl. Med. Mol. Imaging* **2006**, *33*, 1196–1205.

(39) Harrington, K. J.; Rowlinson-Busza, G.; Syrigos, K. N.; Uster, P. S.; Abra, R. M.; Stewart, J. S. W. Biodistribution and pharmacokinetics of111In-DTPA-labelled pegylated liposomes in a human tumour xenograft model: implications for novel targeting strategies. *Br. J. Cancer* **2000**, *83*, 232–238.

(40) Novakova, K.; Laznicek, M.; Rypacek, F.; Machova, L. I-125-labeled PLA/PEO block copolymer: biodistribution studies in rats. *J. Bioact. Compat. Polym.* **2002**, *17*, 285–296.

(41) Wang, H. E.; Yu, H. M.; Lu, Y. C.; Heish, N. N.; Tseng, Y. L.; Huang, K. L.; Chuang, K. T.; Chen, C. H.; Hwang, J. J.; Lin, W. J.; Wang, S. J.; Ting, G.; Whang-Peng, J.; Deng, W. P. Internal radiotherapy and dosimetric study for 111In/177Lu-pegylated liposomes conjugates in tumor-bearing mice. *Nucl. Instrum. Methods* **2006**, *569*, 533–537.

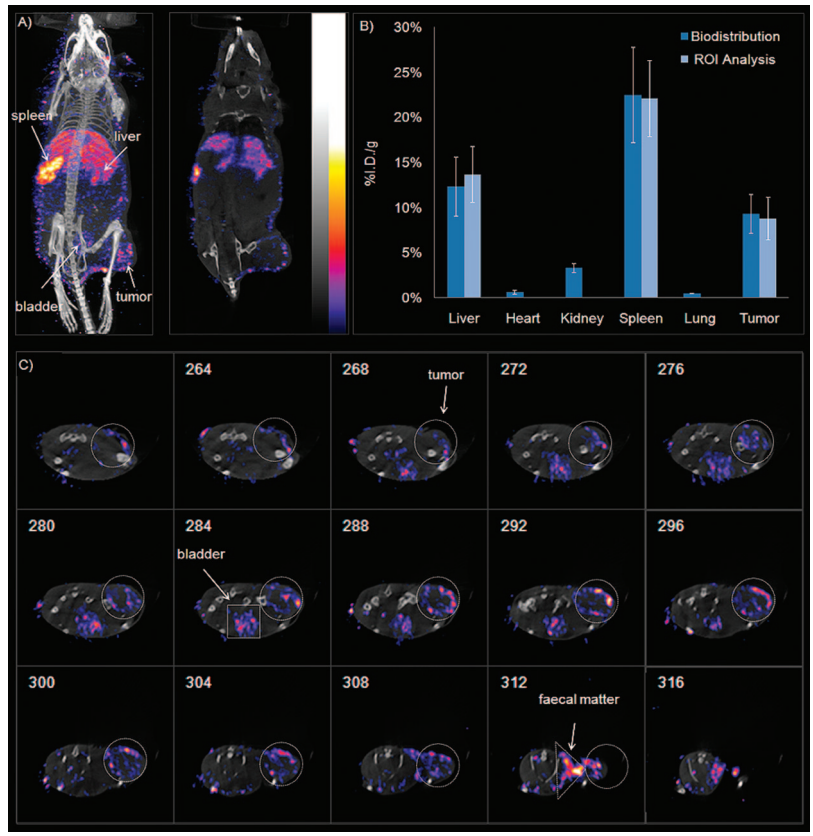

Figure 6. (A) MIP and sagittal image of tissue accumulation of ^{111}In-micelles 48 h p.i in an athymic BALB/c mouse bearing an MDA-MB-231 tumor xenograft after iv administration of ^{111}In-micelles. Clear visualization of the liver, spleen, bladder and tumor was observed. (B) Tissue distribution of ^{111}In-micelles acquired via conventional methodology and MicroSPECT/CT ROI analyses in MDA-MB-231 tumor-bearing mice at 48 h p.i. (C) Transversal slices of tumor accumulation illustrating nonhomogeneous distribution of ^{111}In-micelles.

was observed for ^{111}In-Bn-DTPA (Figure 5C). Tissue accumulation was strongly correlated between ROI analysis and postimaging assessment of biodistribution in the liver and the spleen ($r = 0.91$, $P = 0.02$). Furthermore, as the ^{111}In-micelles were sequestered and eliminated via the MPS (liver and spleen), the radioactivity remaining in circulation (passing through the heart) was noticeably diminished while the activity in the liver and spleen was increased (Figure 5E).

MicroSPECT/CT Imaging in Mice Bearing MDA-MB-231 Tumor Xenografts. As shown in Figures 6A and 6B, accumulation of radioactivity in the spleen, liver, and tumor was observed at 48 hpi of ^{111}In-micelles in athymic mice bearing s.c. MDA-MB-231 breast cancer xenografts. Closer examination of the tumor radioactivity on the transverse slices revealed incomplete and nonhomogeneous distribution of ^{111}In within the tumor nodule, with the majority located at the periphery (Figure 6C). Tumor accumulation estimated by ROI analysis was found to be $9 \pm 2\%$ i.d./g. Postimaging quantification of normal tissue and tumor accumulation by γ-counting is shown in Figure 6B. Liver uptake was $13 \pm 3\%$ i.d./g, while spleen uptake was $22 \pm 5\%$ i.d./g. Tumor uptake was found to be $9 \pm 2\%$ i.d./g. These values agreed well with the ROI analysis estimates ($r = 0.91$, $P = 0.03$). Elimination kinetics from the blood was very rapid for the ^{111}In-Bn-DTPA and no distinguishable localization in the MDA-MB-231 tumor xenografts was observed at 48 h p.i. In contrast, the ^{111}In-micelles exhibited 52-fold significantly greater tumor accumulation (9 vs 0.17% i.d./g) that was clearly visualized on the images. Maximal tumor uptake was observed at 48 h p.i., and ROI analysis again correlated well with conventional postimaging biodistribution data measured by γ-counting ($r = 0.91$ and $P = 0.03$).

Discussion

With numerous drug formulations based on block copolymer micelles in clinical evaluation for the treatment of cancer, there exists a need to develop imageable micelle formulations that enable noninvasive image-based assessment of the pathway and fate of these systems *in vivo*. The radiolabeling of block copolymer micelles with ^{111}In enables high resolution SPECT imaging which when combined with CT provides information on the location of the micelles in the context of the whole body frame. In terms of spatial resolution, sensitivity, and potential for quantification, the combination of SPECT and CT is particularly powerful.[42]

Moreover, the integration of nuclear imaging, such as SPECT, and nanotechnologies is expected to expedite the acquisition of their PK and biodistribution in preclinical and clinical studies. In particular, the pharmacological disposition

of the nanotechnology including its adsorption, distribution, and elimination can be monitored in real-time in a noninvasive manner. For instance, drawing ROI over the heart and other organs affords accurate quantification of the concentrations of agents in blood and tissue. Several preclinical studies have shown that ^{111}In concentrations in tissues can be delineated with acceptable accuracy using microSPECT imaging.[43,44] However, there are inherent limitations associated with ROI analysis to quantify the distribution of ^{111}In in tissues. For example, only radioactivity in visibly distinguishable organs and tissues can be quantified, and drawing the ROI on the images is somewhat subjective. In addition, the accuracy of quantification of ^{111}In uptake in organs by ROI image analysis can be influenced by scattered γ-photons (partial volume effect) and attenuation by overlying tissues (negligible in a mouse model but much greater in humans). As well, longitudinal assessment of ^{111}In distribution by microSPECT imaging is limited by the half-life of the radionuclide (i.e., $t_{1/2}$ ^{111}In = 2.83 days). Nevertheless, a significant correlation between microSPECT/CT ROI analysis and the biodistribution data obtained by γ-counting of excised tissues in healthy ($r = 0.93$, $P = 0.001$) and tumor-bearing mice ($r = 0.91$, $P = 0.03$) was established in this study, implying that imaging can be used as a noninvasive tool to accurately quantify relative tissue concentrations of ^{111}In-micelles.

The high sensitivity and submillimeter resolution of microSPECT/CT enables noninvasive assessment of the efficacy or tissue toxicity of ^{111}In-labeled systems for tumor diagnosis or treatment. Due to the modular design of the block copolymer micelles, changes to the copolymer composition may be made based upon imaging studies to circumvent problems such as toxicity, poor stability, or low tumor localization. For example, it is evident that there is significant liver and spleen accumulation of the ^{111}In-micelles. Based on this, optimization strategies can be employed to reduce uptake in these organs. One strategy could be to replace or modify the metal chelator SCN-Bn-DTPA employed in this study. In comparative biodistribution studies of five different backbone substituted derivatives of SCN-Bn-DTPA linked to a monoclonal antibody (mAb) and labeled with ^{111}In, Roselli et al. found that the mAb-1B3M-DTPA had a tumor to liver ratio of 9.96 in comparison to 3.99 for mAb-SCN-Bn-DTPA at 120 h p.i., respectively in athymic mice bearing a human colon carcinoma xenograft.[45] Furthermore, they found that tumor uptake increased 2-fold from 20.67 to 41.7% i.d./g after 120 h with the mAb-1B3M-DTPA derivative in comparison to the mAb-SCN-Bn-DTPA.[45] Similarly, active delivery to tumor-associated epitopes overexpressed on cancer cells via conjugation of a targeting moiety to the surface of delivery systems can result in significantly higher tumor uptake.[46] In this way, modification of the PEG-*b*-PCL micelle surface with epidermal growth factor (EGF) or trastuzumab (Herceptin) to route the micelles to EGFR or HER2-positive breast cancer could be a means of enhancing and increasing the specificity of tumor accumulation. The use of such targeting ligands could also inform on the expression of tumor status indicators such as tumor cell surface receptors or tumor vasculature markers which would provide valuable insight into the metastatic potential, angiogenic activity and possible drug resistance of the tumor. Through imaging, this invaluable information will enable the development of personalized treatment strategies.[47]

Importantly, in the current study microSPECT imaging of ^{111}In-micelles provided insight on the intratumoral distribution of these nanoassemblies *in vivo*. Specifically, analysis of the transverse slices of the tumor revealed heterogeneous distribution and incomplete tumor penetration of the ^{111}In-micelles (Figure 6C). The heterogeneity could be associated with the disorganization of the tumor vasculature[48] and the limited penetration of the micelles from the vascular surface into the tumor interstitium. Therefore, despite the significant accumulation of the micelles at the tumor site via passive targeting, the distribution of the delivery system is limited primarily to the tumor periphery. This critical information, that is otherwise unavailable through traditional assessment of biodistribution, could have profound implications in terms of the ability of such a micelle formulation to eradicate all or most tumor cells in a lesion. To date, evaluation of the relationships between properties of nanocarriers and their performance *in vivo* has largely been performed using traditional methods. Therefore, information on the intratumoral distribution of delivery systems is limited. A recent study that relied on intravital laser-scanning confocal microscopy of solid tumors in nude mice

(42) Zheng, J.; Jaffray, D.; Allen, C. Nanosystems for multimodality in vivo imaging. In *Multifunctional Pharmaceutical Nanocarriers*; Torchilin, V. P., Ed.; Springer:in press.

(43) Carlson, S. K.; Classic, K. L.; Hadac, E. M.; Bender, C. E.; Kemp, B. J.; Lowe, V. J.; Hoskin, T. L.; Russell, S. J. In vivo quantitation of intratumoral radioisotope uptake using micro-single photon emission computed tomography/computed tomography. *Mol. Imaging Biol.* **2006**, *8*, 324–332.

(44) Vemulapalli, S.; Metzler, S. D.; Akabani, G.; Petry, N. A.; Niehaus, N. J.; Liu, X.; Patil, N. H.; Greer, K. L.; Jaszczak, R. J.; Coleman, R. E.; Dong, C.; Goldschmidt-Clermont, P. J.; Chin, B. B. Cell therapy in murine atherosclerosis: in vivo imaging with high-resolution helical SPECT. *Radiology* **2007**, *242*, 198–207.

(45) Roselli, M.; Schlom, J.; Gansow, O. A.; Brechbiel, M. W.; Mirzadeh, S.; Pippin, C. G.; Milenic, D. E.; Colcher, D. Comparative biodistribution studies of DTPA-derivative bifunctional chelates for radiometal labeled monoclonal antibodies. *Nucl. Med. Biol.* **1991**, *18*, 389–394.

(46) Elbayoumi, T. A.; Torchilin, V. P. Enhanced accumulation of long-circulating liposomes modified with the nucleosome-specific monoclonal antibody 2C5 in various tumours in mice: gamma-imaging studies. *Eur. J. Nucl. Med. Mol. Imaging* **2006**, *33*, 1196–1205.

(47) Koning, G. A.; Krijger, G. C. Targeted multifunctional lipid-based nanocarriers for image guided drug delivery. *Anti-Cancer Agents Med. Chem.* **2007**, *7*, 425–440.

(48) Pasqualini, R.; Arap, W.; McDonald, D. M. Probing the structural and molecular diversity of tumor vasculature. *Trends Mol. Med.* **2002**, *8*, 563–571.

implanted with a dorsal skin fold window chamber, showed that macromolecular carriers with molecular weights of 40, 70 and 2000 kDa and 2000 kDa (i.e., hydrodynamic diameters of ~11, 15 and 50 nm, respectively) had moderate to long circulation lifetimes, yet the apparent tumor permeability rates decreased almost 6-fold; from $9.5-9.8 \times 10^{-7}$ cm/s for the 11 and 15 nm macromolecules to 1.7×10^{-7} cm/s for the 50 nm macromolecules.[26] In order to address the poor tumor penetration of the ^{111}In-micelles achieved in this study, the copolymers could be tailored to form smaller micelles which may in turn facilitate increased tumor permeability. These studies highlight the key information that may be obtained through noninvasive image-based assessment of the distribution of drug formulations.

The findings from this study support the use of radiolabeled block copolymer micelles for image-guided drug delivery. Multifunctional block copolymer micelles labeled with ^{111}In and loaded with a therapeutic agent would allow for real-time monitoring of the tumor accumulation and intratumoral distribution of the formulation. However, use of this approach to achieve image-guided therapy requires that the majority of the drug remain within the carrier until reaching its target site. Information obtained through image-guided drug delivery is critical to achieving leap-step advances that result in more efficacious treatments and the future realization of personalized medicine. In the clinical translation of these advanced drug delivery vehicles, such information could provide insight into why some formulations, though promising in preclinical animal models, fail in clinical development. Imageable drug delivery vehicles could allow for patient prescreening for early optimization of the dose or dose schedule and enable identification of individual patients with high tumor accessibility prior to administration of a drug-loaded formulation. This would enable the differentiation of patients more likely to respond to drug treatment from patients that are less likely to respond. Alternative treatment strategies could then be pursued for patients that are less likely to respond.

In closing, the full exploitation of block copolymer micelles as a delivery technology for drugs or radionuclides requires a firm understanding of their pathway and fate *in vivo*. The integration of advances in imaging (i.e., hybrid MicroSPECT/CT) and radiochemistry (i.e., p-SCN-Bn-DTPA) with this delivery technology allowed for the development of an imaging agent (i.e., ^{111}In-micelles) that was evaluated *in vivo* with high sensitivity and high resolution. MicroSPECT/CT imaging allowed for accurate visualization and quantification of the tissue distribution and fate of the ^{111}In-labeled micelles *in vivo* in real time in the same animal. Furthermore, microSPECT/CT imaging enabled the quantification of the nonspecific tumor uptake of the micelles and visualization of their degree of tumor penetration. In this way, the image-based assessment provided unique information that is not obtainable using conventional methodologies.

Acknowledgment. This study was supported by grants from the Canadian Institutes of Health Research, Canadian Breast Cancer Research Alliance and Ontario Institute for Cancer Research 1 mm Challenge Program to C.A. and R.M.R. as well as an MDS-Nordion Graduate Scholarship in Radiopharmaceutical Sciences to B.H. The authors thank Deborah Scollard for her assistance in the *in vivo* experiments.

Supporting Information Available: Details of physicochemical characterization including FTIR analysis of NH_2-PEG-*b*-PCL copolymers, purification of unbound SCN-Bn-DTPA by SEC, ITLC analysis of DTPA conjugation efficiency and radiochemical purity, and *in vitro* characterization of serum stability. This material is available free of charge via the Internet at http://pubs.acs.org.

MP8002418